Corrosion of Hot Dip Galvanized Rebars in Concrete under the Attack of Chlorides and Freeze-Thaw Cycles

By A. Hegyi [1, 2], H. Vermesan [1], V. Rus [1], E. Grünwald [1], G. Vermesan †

[1] Technical University, Faculty of Materials Science and Engineering, Cluj – Napoca, România

[2] National Institute for Research and Development in Construction, Urban Planning and Sustainable Spatial Development "Urban-Incerc", Cluj – Napoca, România

Dieser Aufsatz präsentiert ein mathematisches Modell zur Simulation physikalischer Phänomene, die bei der Korrosion von feuerverzinkten Bewehrungsstäben auftreten, im Vergleich mit unbehandelten Stahlbewehrungen in Beton unter dem Einfluss von Chloriden und Frost-Tau-Wechseln. Dazu werden das physikalische und das korrespondierende mathematische Model sowie das Gleichungssystem mit den Anfangs- und Randbedingungen vorgestellt. Das zugehörige numerische Modell und die numerischen Methoden der Diskretisierung des Differentialgleichungssystems, auf dem das mathematische Modell basiert, werden ebenfalls behandelt. Die folgenden Parameter wurden dabei berücksichtigt: die Feuchtigkeit des Betons, der Gehalt an Chlorid-Ionen und die Änderungen der Temperatur. Der Zeitraum bis zum Einsatz der Korrosion, die Abnahme des Durchmessers der Bewehrungsstäbe, die Ausbreitung der Korrosionsprodukte und die Variation des Korrosionsstroms wurden unter den obwaltenden Umweltbedingungen, der Einwirkungszeit und des Typs der verwendeten Bewehrungsstäbe bestimmt.

This paper presents a mathematical model for the simulation of physical phenomena that appear in the hot dip galvanized rebars corrosion process, compared with the bare steel rebar in concrete, under the attack of chlorides and freeze-thaw cycles. The physical and corresponding mathematical model are presented and the system of governing equations along with initial and boundary conditions were established. The associated numerical model and the numerical methods of discretization and solving the differential equations system on which the mathematical model is based are also presented. The following parameters were considered: concrete humidity, chloride ions content and temperature variation. The time until corrosion initiation, rebar's diameter reduction, the advance of the corrosion products front and corrosion current variation were determined, according to environment conditions, exposure time and type of rebar used.

1 Introduction

Reinforcement corrosion due to the presence of chlorine can be divided in three distinct phases. The first phase is represented by the gradual penetration of chlorine through diffusion from the surface of the concrete to the steel-concrete interface. The second phase starts with the initiation of the corrosion process, at $t = t_{initiation}$, and it is characterized by the expansion of rust and emersion of the transition area between steel and concrete. When the open spaces formed in the transition area are completely filled up by rust, further accumulation of rust will cause the appearance of cracks in the adjacent concrete layers at $t = t_{stress}$, the moment which indicates the beginning of the third phase. During this final phase, the cracks expand to the layers of concrete surrounding the reinforcement, until they reach the external surface of the part, or cause other levels of deterioration. This moment, $t = t_{spalling}$, indicates the end of the third phase.

The first phase is the longest and depends mostly on factors such as: the reinforcement's resistance to corrosion, the thickness and quality of the concrete, the precautions taken when fabricating the reinforced concrete and the environmental conditions. The second phase is shorter than the first and is

determined by the porosity of the transition area and the corrosion speed of the reinforcement. The third phase is the shortest, because the cracks that appeared due to rust expansion spread quickly through the concrete. The service time of the reinforced concrete structures can be defined as the sum of these three phases [6].

In order to increase the durability of reinforced concrete structures, the reinforcement itself must be able to resist chlorine-induced corrosion. Therefore, by using hot dip galvanized steel reinforcement, the structure is protected against corrosion due to the fact that the minimal chlorine level in order to initiate the corrosion process must be 2.5 to 4 times higher than with plain steel, it takes longer for the corrosion process to affect the zinc layer which grants the structure cathodic protection by becoming an anode and sacrificing itself in order to protect the iron against corrosion, thus ensuring that the structure may be used for a longer period of time until the layer of zinc is fully consumed.

2 Experiment

In order to explore the deterioration process of steel reinforcements in reinforced concrete structures investigation experiments were performed on cubic concrete samples with the edge length of $L = 150$ mm, in which a steel reinforcement was inserted vertically and centered, with the diameter of $D_p = 8$ mm. The experiment was conducted using both plain steel, as well as hot dip galvanized steel. The thickness of the zinc coating was determined experimentally at an average of 140 µm.

After manufacturing, the reinforced concrete samples were kept for maturation under laboratory conditions for 28 days.

A series of 4 samples containing hot dip galvanized reinforcement and 4 samples with plain steel reinforcement were tested in order to determine the adherence between the reinforcement and the concrete 28 days after the manufacturing, while kept under laboratory conditions all this time. This series is considered to be the control sample.

The other samples, containing both galvanized and plain steel reinforcements, were divided into 4 series, as shown in *Figure 1*, and were subjected to aggressive environmental conditions: immersion in 3 % NaCl solution for 25 days, respectively 100 days and 25 cycles, and 100 freeze – thaw cycles. The latter implies freezing the sample by maintaining it at a temperature of –20 °C for 4 hours, and then thawing it by immersing it in a 3 % NaCl solution at 23 °C for another 4 hours, and then maintained for 16 hours in the laboratory, at a temperature of 23 °C and 75 % relative air humidity.

Concrete reinforcement matrix adhesion was determined by pull-out method, both for specimens kept in laboratory conditions and subjected to the aggressive environment (immersion in 3 % NaCl solution or freeze-thaw cycles).

For every sample, the maximum pulling strength σ_{max} was calculated. The highest average pulling strength, σ_{max} is the arithmetic mean of the maximum pulling strength individual values.

For the concrete samples with plain steel reinforcement, matured for 28 days under laboratory conditions and then kept for 25, respectively 100 days in corrosive environment, the percentual reduction of the concrete-reinforcement adhesion PA (%) was calculated, in relation to the average adhesion determined for the plain steel control sample. The percentual reduction of the concrete-galvanized reinforce-

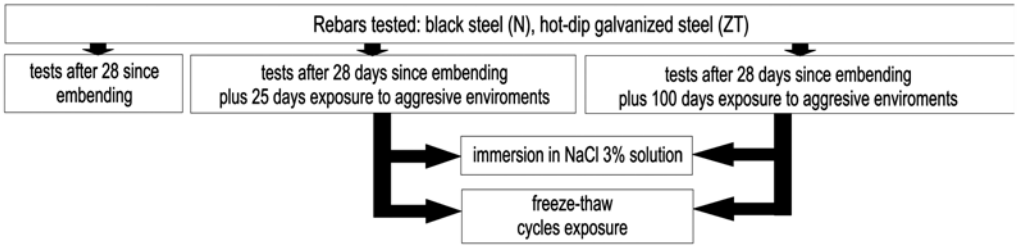

Fig. 1: The distribution of the samples subjected to testing

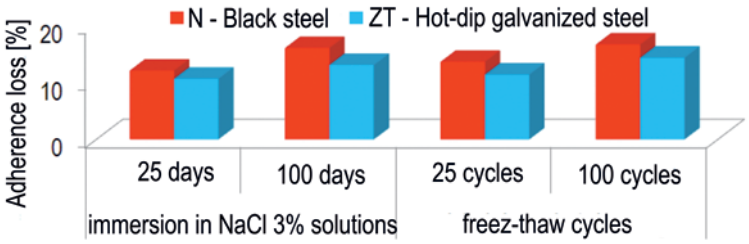

Fig. 2: The percentual reduction of the concrete-reinforcement adhesion PA (%), in relation to the medium adhesion determined for the control sample

ment adherence was calculated in a similar manner, in relation to the average adherence determined for the galvanized steel control sample. The results are presented in *Figure 2*.

3 Mathematical modeling of corrosion in reinforced concrete

3.1 The mathematical model

For establishing the corresponding mathematical model of the process, the cubic sample is placed in the positive quadrant of the Xyz coordinates system. The axes Ox, Oy and Oz are parallel to the edges of the cubic sample, and one of the base corners coincides with the origin of the system, O.

The main physical phenomena that influence the process of reinforced concrete deterioration and corrosion of the steel reinforcements are: heat transfer and temperature expansion/contraction, humidity diffusion and humidity expansion or an increase in porosity due to a decrease in humidity, carbon dioxide diffusion followed by the carbonation of concrete and the diffusion of chlorides, which upon accumulating at the steel – concrete interface may cause the corrosion of the steel. These physical and chemical events that accelerate the deterioration of the reinforced concrete structures may generate and build up certain local strains in the concrete, that lead to the formation, growth and expansion of cracks in the concrete. In this case, the carbonation process was neglected.

The time – space evolution of temperature and the humidity and chlorine diffusion are controlled by the corresponding equations, which are based on fundamental principles of physics, expressed as humidity conservation conditions, chlorine content and thermal characteristics. In the Xyz system of coordinates we have the equation system which consists of Fourier's equation for heat transfer and Fick's second law, modified, to calculate the humidity diffusion and the chloride content of the concrete. These are presented in equations <1> to <3>:

$$\rho c\frac{\partial T}{\partial t}=\frac{\partial}{\partial x}\left(k\frac{\partial T}{\partial x}\right)+\frac{\partial}{\partial y}\left(k\frac{\partial T}{\partial y}\right)+\frac{\partial}{\partial z}\left(k\frac{\partial T}{\partial z}\right)+\dot{Q}(t) \quad <1>$$

$$\frac{\partial w}{\partial t}=\frac{\partial}{\partial x}\left(D\frac{\partial w}{\partial x}\right)+\frac{\partial}{\partial y}\left(D\frac{\partial w}{\partial y}\right)+\frac{\partial}{\partial z}\left(D\frac{\partial w}{\partial z}\right)+\dot{Q}_m(t) \quad <2>$$

$$\frac{\partial C_{LF}}{\partial t}=\frac{\partial}{\partial x}\left(D_{cl}\frac{\partial C_{LF}}{\partial x}\right)+\frac{\partial}{\partial y}\left(D_{cl}\frac{\partial C_{LF}}{\partial y}\right)+\frac{\partial}{\partial z}\left(D_{cl}\frac{\partial C_{LF}}{\partial z}\right)-\frac{1}{\omega_e}\frac{\partial C_{LB}}{\partial t} \quad <3>$$

where

T = the temperature in Kelvin degrees [K]
w = humidity content [m^3/m^3 – humidity cubic meter/concrete cubic meter]
C_{LF} = free chlorine content [m^3/m^3 – free chlorine cubic meter/pore humidity cubic meter]
k = thermal conductivity of the material (concrete, steel, zinc) [$W/m\cdot{}^0K$]
ρ = density of material [kg/m^3]
c = specific heat capacity at constant pressure [$J/kg\cdot{}^0K$]
D = moisture diffusion coefficient [m^2/s]
D_{cl} = free chlorine diffusion coefficient [m^2/s]
C_{LB} = bonded chlorine content [kg/m^3]
ω_e = saturation moisture content [m^3/m^3 – moisture cubic meter/concrete cubic meter]

X, y and z represent the interdependent space variables, and t represents the time [s].

The variables $\dot{Q}(t)$ and $\dot{Q}_m(t)$ are the negative or positive source for the heat flux and moisture content.

The equation system <1> to <3> is completed by the relation between the temperature variation and the associated mechanical deformation $\varepsilon_{thermal}$ <4>

$$\varepsilon_{thermal} = \alpha \cdot \Delta T \quad <4>$$

where α represents the coefficient of thermal expansion [K];

and the relation between the variation of moisture content and the associated mechanical deformation – expansion if humidity is rising and contraction if humidity is decreasing $\varepsilon_{shrinkage}$:

$$\varepsilon_{shrinkage} = \beta \cdot (w - w_0) \quad <5>$$

where

β = coefficient of hydration [m^3/m^3 – concrete cubic meter/moisture cubic meter]

w_0 = initial moisture content [m^3/m^3]

The equation system is also completed by the steel corrosion model based on Faraday's law:

$$\frac{dM_s}{dt} = \frac{I_{corr} \cdot A}{n \cdot F} \quad <6>$$

where

M_s = steel mass/steel and zinc mass (in hot dip galvanized reinforcements) consumed during the corrosion process [g]

I_{corr} = electric intensity which passes through the electrochemical cell that produces the corrosion [A]

A = atomic weight of the corroded ion [g/mol]

F = Faraday's constant

n = valence

The initial conditions are those used for the laboratory experiments as presented in *chapter 2*:

$$\begin{cases} T(x,y,z,0) = T_0(x,y,z) \\ w(x,y,z,0) = w_0(x,y,z) \\ C_{LF}(x,y,z,0) = C^0_{LF}(x,y,z) \end{cases} \quad <7>$$

where $T_0(x, y, z)$, $w_0(x, y, z)$, and $C^0_{LF}(x, y, z)$ are the temperature, moisture content and chloride content at the initial moment, at the coordinates occupied by the concrete sample and its surroundings.

At the concrete-air and concrete-reinforcement interfaces, boundary conditions were imposed. Therefore, at the concrete-air interface, at the moment t, we have the boundary conditions as presented in the system <8> [5, 13].

$$\begin{cases} k\dfrac{\partial T(x,y,z,t)}{\partial n} = T_{amb}(x,y,z,t) \\ D\dfrac{\partial w(x,y,z,t)}{\partial n} = w_{amb}(x,y,z,t) \\ D_{cl}\dfrac{\partial C_{LF}(x,y,z,t)}{\partial n} = C_{LF\,amb}(x,y,z,t) \end{cases} \quad <8>$$

where the index amb indicates the dependent variables' value in the environment the cubic sample is placed (air or 3 % NaCl solution), at the moment t and $\partial/\partial n$ indicates the derivative in the normal direction at the concrete-air interface.

The boundary conditions for the thermal field at the concrete-steel, concrete-zinc and zinc-steel interfaces are obtained by equaling the thermal fluxes, as shown in equation <9>.

$$k_1\frac{\partial T_1}{\partial n} = k_2\frac{\partial T_2}{\partial n} \quad <9>$$

where the indexes represent the two separate surroundings, $\vec{n} = (n_x, n_y, n_z)$ and represents the unit normal of the interface. Analog relations are used for the terms w and CLF.

3.2 The numeric model

The numeric model associated with the mathematical model [11, 12] is obtained by discretizing the differential equations system <45–50> and the corresponding conditions, both initial and boundary. To obtain this discretization, the control volume method was used [12].

The space occupied by the cubic sample and the reinforcement is divided into cubic cells with an edge length of dx = dy = dz = 0,002 mm. In order to simulate the processes that occur at the concrete-air interface, the computational domain was extended with an extra layer of air, the thickness of which is equal to the

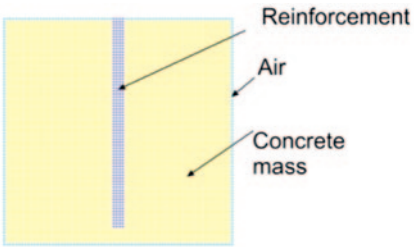

Fig. 3: Vertical section through the center of the reinforced concrete sample, indicating the alignment of the discretization cells in the environment (green), concrete (yellow) and steel(blue)

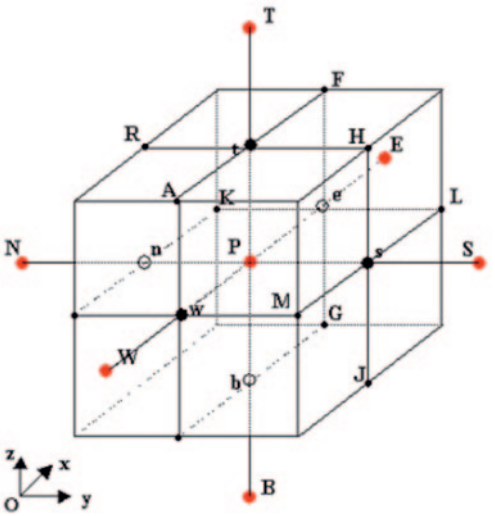

Fig. 4: The elemental cell with the center P

edge length of one cell. A vertical section parallel to the xOz coordinates plane driven through the center of the cubic sample is shown in *Figure 3.* The cells shown in yellow represent the concrete and the color blue represents the reinforcement. In order to apply the boundary conditions at the concrete-environment interface, a layer of air was added, represented by the color green. The humidity content conservation conditions, the chlorine and heat level of each cell is in direct link with the adjacent cells, that are in turn influenced by the present cell. The center point *P (Fig. 4)* is representative for the measurements ρ, T, w, C_{CL}, c, k, D and D_{cl} through the whole cell.

The cells that form the network contain several different materials such as air, concrete, steel, zinc, NaCl solution, therefore an extra variable must be introduced: a tridimensional matrix, meant to control the content of the cells. By using the following notations for its elements obs[i,j,k], (i,k) ε {1,2,…,im} x {1,2,…jm} x {1,2,…,km}, the component from the matrix corresponding to the current cell will have values between 1 and 5, indicating its content: obs[i,j,k] = 1 for cells that contain concrete; obs[i,j,k] = 2 for cells that contain steel; obs[i,j,k] = 3 for cells that contain air; obs[i,j,k] = 4 for cells that contain zinc; obs[i,j,k] = 5 for cells that contain NaCl solution.

For the temporal discretization, an implicit Euler method was used, with the variable time step dt.

The main equations system was integrated on the network cells unlike the usual developments applied in the Taylor series which are used in the classic finite differences methods [12]. For a dependent variable, numerical integration of $\Phi \in \{T, w, C_{LF}\}$ the corresponding differential equations leads to the following algebraic equation:

$$a_p \Phi_p = a_0 \Phi_0 + a_E \Phi_E + a_w \Phi_w + a_T \Phi_T + a_B \Phi_B + a_S \Phi_S + a_N \Phi_N + b \quad <10>$$

where $a_0 = r_0 V_0/dt$, r_0 and V_0 are the density and the volume of the cell centered in P at the previous time step, and dt is the time step measure unit. The a_E, a_W, a_T, a_B, a_S and a_N coefficients contain the sum of the diffusive contributions of the adjacent cells. This diffusive component has the general form $G_f A/d_n$ where A is the area of the common side between the current and adjacent cell, and dn is the distance between the centers of the two cells. The exchange coefficient for the interface between the two cells, G_f, is calculated as an arithmetic average for the density and specific heat, and as an harmonic averagefor the thermal conductivity from the adjacent central nodes.

3.3 Discretization of the heat conservation equation

$$\dot{Q}(t) = -\frac{L_w}{2\Delta_f} \rho_w w \frac{\partial T}{\partial t} \cdot I \quad <11>$$

where L_W = 2 500 000 J/kg, ρ_W is the moisture content density [kg/m^3], I is an indicator which may have the values 0 or 1, and Δ_f is a constant used to simulate a gradual release of the latent heat – not instantaneous – when temperature decreases below freezing point T_f. So:

$$I = \begin{cases} 1 & pentru \quad T_f - \Delta_f <= T(x,y,z,t) <= T_f + \Delta_f \\ 0 & pentru \quad |T(x,y,z,) - T_f| > \Delta_f \end{cases} \quad <12>$$

Bažant and colab. [1], propose Δ_f = 1 ºK. Due to <11>, there is a connection between the heat transfer and the moisture transfer, thus by replacing $\dot{Q}(t)$ resulted in equation <1>, we obtain:

$$\rho \bar{c} \frac{\partial T}{\partial t} = \frac{\partial}{\partial x}\left(k \frac{\partial T}{\partial x}\right) + \frac{\partial}{\partial y}\left(k \frac{\partial T}{\partial y}\right) + \frac{\partial}{\partial z}\left(k \frac{\partial T}{\partial z}\right) \quad <13>$$

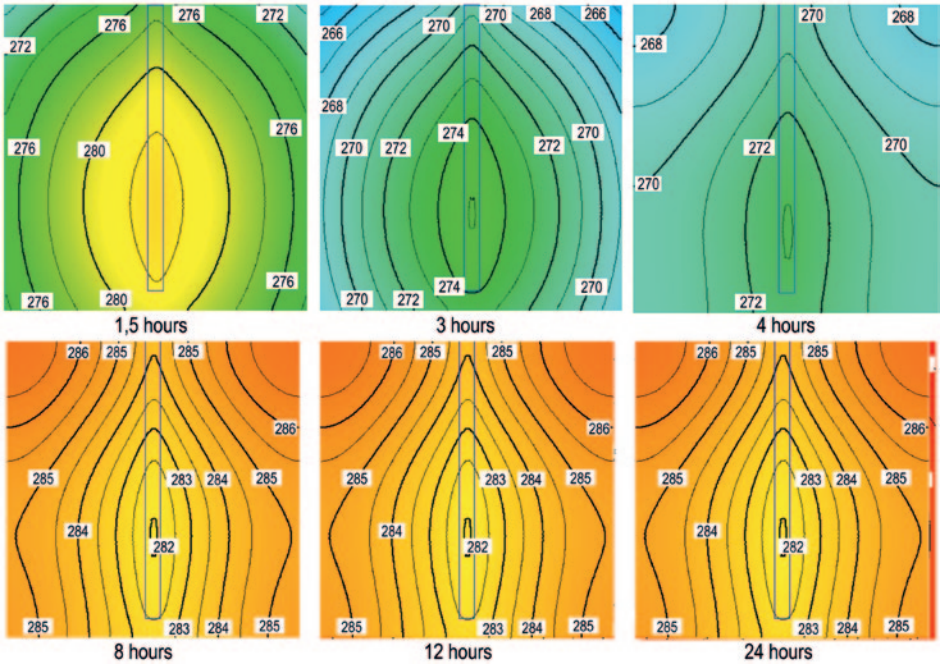

Fig. 5: Evolution of the thermal field in the cross section of the cubic sample during a freeze-thaw cycle

Where $\overline{c}$ represents the „modified" specific heat, or equivalent.

$$\overline{c} = c + \frac{L_w}{2\Delta_f}\frac{\rho_w}{\rho} wI \qquad <14>$$

Which is a function that depends on time and space due to the factor w.

The standard discretized form used in the volume control method is [12].

$$a_P T_P = a_P^0 T_P^0 + a_E T_E + a_W T_W + a_N T_N + a_S T_S + a_T T_T + a_B T_B$$

In *Figure 5* we have the evolution of the thermal field in the cross section of the cubic sample during a freeze-thaw cycle.

3.4 Discretization of the moisture conservation equation

The discretized form of equation <2> is obtained in a similar manner for the diffusion of the moisture content, where the source term $\dot{Q}_m(t)$ (which represents the generation of a moisture content due to the carbonation reactions, or water consumption during the hydrating reactions [3]) was neglected.

$$am_P w_P = am_P^0 w_P^0 + am_E w_E + am_W w_W + am_N w_N + am_S w_S + am_T w_T + am_B w_B \qquad <15>$$

where

$$\begin{cases} am_E = \frac{D_e}{dx}dydz \quad , \quad am_W = \frac{D_w}{dx}dydz \\ am_N = \frac{D_n}{dy}dxdz \quad , \quad am_S = \frac{D_s}{dy}dxdz \\ am_T = \frac{D_t}{dz}dxdy \quad , \quad am_B = \frac{D_b}{dz}dxdy \\ am_P^0 = \frac{V}{dt} \\ am_P = am_P^0 + am_E + am_W + am_N + am_S + am_T + am_B \end{cases} \qquad <16>$$

The diffusion coefficient D is greatly dependent on both the relative moisture content in the pores, and the temperature. Xi and colab. [15] formulated this relationship as following:

$$D(h) = A\left\{\theta + \psi\left[1 - 2^{-10^{\gamma(h-1)}}\right]\right\} \qquad <17>$$

where

h = relative humidity

A = $7.0 \cdot 10^{-10}$ m²/s

θ = 0.05

ψ = 0.4

γ = 4

Figure 6 shows the humidity front progression in the central section of the cubic sample during the first freeze-thaw cycle.

3.5 Discretization of chlorine content conservation equation

Equation <3> can be rewritten as [14]:

$$\frac{\partial C_{LF}}{\partial t} = \frac{\partial}{\partial x}\left(D^* \frac{\partial C_{LF}}{\partial x}\right) + \frac{\partial}{\partial y}\left(D^* \frac{\partial C_{LF}}{\partial y}\right) + \frac{\partial}{\partial z}\left(D^* \frac{\partial C_{LF}}{\partial z}\right) \quad <18>$$

where D^* is the effective diffusivity – also called apparent diffusivity – of chlorine in concrete. As such, the discretized form of the equation will be:

$$ac_P C_{LF,P} = ac_P^0 C_{LF,P}^0 + ac_E C_{LF,E} + ac_W C_{LF,W} + ac_N C_{LF,N} + ac_S C_{LF,S} + ac_T C_{LF,T} + ac_B C_{LF,B} \quad <19>$$

where

$$\begin{cases} ac_E = \dfrac{D_e^*}{dx} dydz \quad , \quad ac_W = \dfrac{D_w^*}{dx} dydz \\ ac_N = \dfrac{D_n^*}{dy} dxdz \quad , \quad ac_S = \dfrac{D_s^*}{dy} dxdz \\ ac_T = \dfrac{D_t^*}{dz} dxdy \quad , \quad ac_B = \dfrac{D_b^*}{dz} dxdy \\ ac_P^0 = \dfrac{V}{dt} \\ ac_P = ac_P^0 + ac_E + ac_W + ac_N + ac_S + ac_T + ac_B \end{cases} \quad <20>$$

The effective diffusivity coefficient shall be

$$D^* = D_{cl}^0 \cdot F_1(C_{LB}) \cdot F_2(t) \cdot F_3(C_{LF}) \cdot F_4(T) \cdot F_5(\rho_{local}) \quad <21>$$

where

$$F_1(C_{LB}) = \frac{1}{1 + \frac{1}{\omega_e}\frac{\partial C_{LB}}{\partial C_{LF}}} \quad <22>$$

where $\partial C_{LB} / \partial C_{LF}$ is the chloride binding capacity of concrete, which is determined based on an isothermal model. In this paper, the Freundlich isothermal model was used [2].

$$\frac{\partial C_{LB}}{\partial C_{LF}} = \alpha_{cl} \cdot \beta_{cl} \cdot C_{LF}^{\beta_{cl}-1} \quad <23>$$

The equation becomes:

$$F_1(C_{LB}) = \frac{1}{1 + \frac{\alpha_{cl} \cdot \beta_{cl} \cdot C_{LF}^{\beta_{cl}-1}}{\omega_e}} \quad <24>$$

For concrete made with Portland cement, the water- cement ratio is 0.4, $D_{cl}^0 = 1.45 \cdot 10^{-12}$ m²/s, and $\alpha_{cl} = 1.037$, $\beta_{cl} = 0.36$ si, $\omega_e = 0.08$ (moisture m³/concrete m³).

The factor $F_2(t)$ from the effective diffusivity equation represents the influence the concrete's age has, and indicates concrete porosity reduction in time due to cement hydratation:

$$F_2(t) = \left(\frac{t_{ref}}{t}\right)^m \quad <25>$$

where t_{ref} is the reference age for which the value D_{cl}^0 was determined, t_{ref} = 1 year, t is the actual age of the concrete [years] and the empirical parameter m = 0.04.

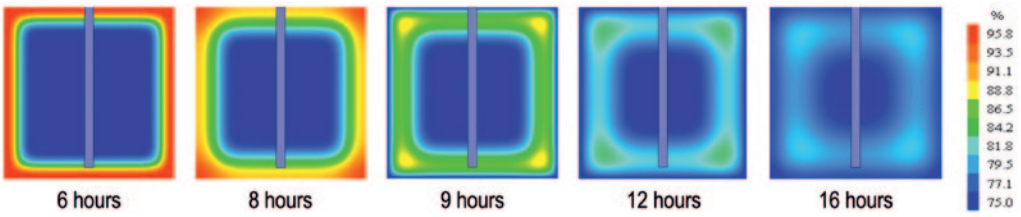

Fig. 6: Humidity front progression in the central section of the cubic sample during the first freeze-thaw cycle

The factor $F_3(C_{LF})$ represents the local chlorine content influence on the effective diffusivity. Xi and Bažant [14] propose

$$F_3(C_{LF}) = 1 - k \cdot (C_{LF})^n \quad <26>$$

where the empirical parameters k and n are: $k = 8.333$ and $n = 0.5$. In regard (95) C_{LF} is expressed in kg/kg (chlorine kg/concrete kg).

The factor $F_4(T)$ represents temperature influence on the effective diffusivity.

Based on Arrhenius's law, it can be expressed as

$$F_4(T) = \exp\left[\frac{E}{R}\left(\frac{1}{T_{ref}} - \frac{1}{T}\right)\right] \quad <27>$$

where E is the activation energy for the chlorine diffusion process. For a water-cement ratio of 0.4, E = 44.6 kJ/mol. R is the gas constant, $R = 8.314$ J/mol, the reference temperature $T_{ref} = 296$ °K, and T is the concrete's current temperature.

$F_5(\rho_{local})$ represents the influence of local relative density of concrete cracking ρ_{local}

$$F_5(\rho_{local}) = (MF - 1) \cdot \rho_{local} + 1 \quad <28>$$

where $MF = 8$, is an empirically determined parameter. *Figure 7* shows the progression of the chlorine ions content for the samples immersed in NaCl 3 % solution for different times after immersion.

3.6 Expansion of the corrosion products model

Plain steel reinforcement

In order to determine the rust expansion model, the simulation proposed by Chen and Mahavedan [4] was used. The most common and significant corrosion products are ferrous hydroxide $Fe(OH)_2$ and ferric hydroxide $Fe(OH)_3$ (red rust). Therefore, to simplify the numeric model, it is assumed that only these two products appear, in relatively equal quantities. Generally, in treatises, the density of the corrosion products is expressed as a fixed fraction of the density of iron:

$$r = \frac{\rho_r}{\rho_s} \quad <29>$$

where ρ_r is the corrosion product density and ρ_s is the density of iron. The values of these densities are: Fe density = 7850 kg/m^3, $Fe(OH)_2$ density = 3500 kg/m^3 and $Fe(OH)_3$ density = 3750 kg/m^3. Therefore, $r = (r_1 + r_2)/2 = 2{,}17$.

According to Faraday's law, equation <6> represents the connection between the iron mass consumed during corrosion M_s and the intensity of the electric current causing the corrosion I_{corr}. Assuming that the valence n of the corrosion product is the average of the $Fe(OH)_2$ and $Fe(OH)_3$ valences, n will be $n = (2 + 3)/2 = 2.5$. So, the equation will become:

$$\frac{dM_s}{dt} = 2.315 \cdot 10^{-4} \cdot I_{corr} \quad <30>$$

from which the value of M_s may be determined, after the corrosion process starts. The corresponding mass of the generated corrosion product M_r will be

$$M_r = \frac{M_s}{r_m} \quad <31>$$

where $r_m = 0.5685$, is the average of the r values for the two corrosion products, $Fe(OH)_2$ and $Fe(OH)_3$.

This equation is representative for corrosion models that imply constant speed for the iron corrosion process, implying a constant rust generation speed.

To create the modelling of rust expansion and its mechanical effects, the following notations were used: D_b represents the initial diameter of the steel bar, D_{rb} is the reduced diameter of the steel bar after corrosion and D_{eb} is the diameter of the rust expansion front *(Fig. 8)*.

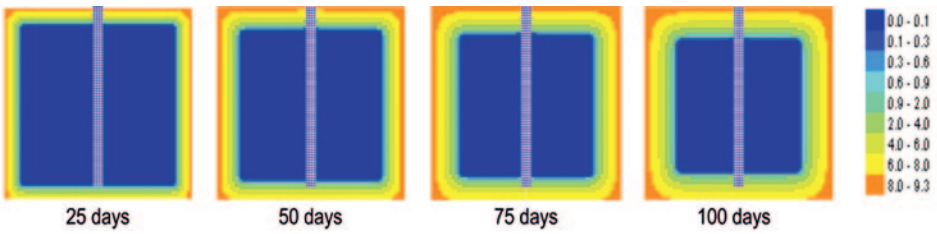

Fig. 7: Distribution of the chlorine content in the central section of the cubic reinforced concrete sample, for t = 25 days, 50 days, 75 days and 100 days since immersion in 3 % NaCl solution

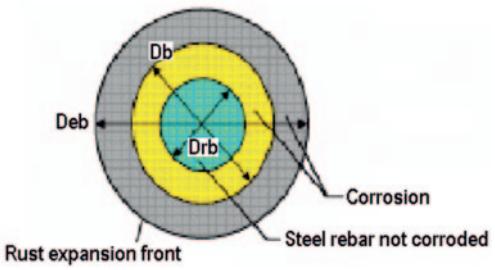

Fig. 8: Rust expansion front generated by corrosion [4]

The corrosion current intensity will be:

$$I_{corr} = \pi \cdot D_{rb} \cdot i_{corr} \cdot L \quad <32>$$

where L is the length of the corroded bar [m], i_{corr} is the corrosion current intensity [A/m^2]. The mass and volume of the consumed iron (due to corrosion of the steel beam), per length unit (L = 1 m), in Δt time will be

$$\Delta M_s = 2.315 \cdot 10^{-4} \cdot \pi \cdot D_{rb} \cdot i_{corr} \cdot \Delta t \quad <33>$$

$$\Delta V_s = \frac{\Delta M_s}{\rho_s} = 2.95 \cdot 10^{-11} \cdot \pi \cdot D_{rb} \cdot i_{corr} \cdot \Delta t \quad <34>$$

where ΔM_s [g/m] and ΔV_s [m^3/m].

The radial expansion in the steel bar will be equal to the difference between the volume of rust generated and the corroded iron volume:

$$\Delta V = \Delta V_r - \Delta V_s = \frac{\Delta M_r}{\rho_r} - \frac{\Delta M_s}{\rho_s} = 8.257 \cdot 10^{-11} \cdot \pi \cdot D_{rb} \cdot i_{corr} \cdot \Delta t \quad <35>$$

The reduced diameter of the steel bar that has not been corroded at time step k, is obtained using the following relation:

$$\Delta V_{s,k} = \pi \frac{D_b - D_{rb,k}}{2} \cdot \frac{D_b + D_{rb,k}}{2} = 2.95 \cdot 10^{-11} \cdot \pi \cdot D_{rb,k} \cdot i_{corr,k} \cdot \Delta t_k \quad <36>$$

After the mathematical processing of the equations, by adding the first n timeframes of the model, we obtained the following:

$$D_{rb,n} = D_b - 5.90 \cdot 10^{-11} \cdot \sum_{k=1}^{n} i_{corr,k} \cdot \Delta t_k \quad <37>$$

Therefore, the reduced diameter of the steel beam after the first n time steps, $D_{rb,n}$ (m) is the sum of the diameter reductions found in time steps Δt_1, …, Δt_n.

In the same manner, the diameter of the radial expansion front $D_{eb,k}$ and the radial translocation of the expansion front u_r at time step n will be

$$u_{rb,n} = \frac{D_{eb,n} - D_b}{2} = D_b + 8.257 \cdot 10^{-11} \cdot \sum_{k=1}^{n} \frac{D_{rb,k}}{D_{eb,k}} \cdot i_{corr,k} \cdot \Delta t_k \quad <38>$$

where $u_{rb,n}$ is expressed in meters.

In order to calculate the corrosion current density i_{corr}, the empirical formula submitted by Liu and Weyers [10] was used:

$$i_{corr} = 0.926 \cdot \exp\left[7.98 + 0.771 \cdot \ln(1.69 \cdot C_{LT}) - \frac{3006}{T} - 0.000116 \cdot R_c + 2.24 \cdot t^{-0.215}\right] \quad <39>$$

where C_{LT} is the total chlorine content [kg/m^3], T is the temperature in (K), R_c is the ohmic resistance of the concrete [ohms], and t is the time passed from the beginning of the corrosion process [years]. In equation <39> i_{corr} is expressed in µA/cm^2.

The total chlorine content ws calculated using the formula

$$C_{LT} = C_{LB} + w \cdot C_{LF} \quad <40>$$

where w is the moisture content [humidity m^3/concrete m^3] and the ohmic resistance is

$$R_c = \exp\left[8.03 - 0.549 \cdot \ln(1 + 1.69 \cdot C_{LT})\right] \quad <41>$$

At the reinforcement/concrete interface's transition zone, a porous area is present, that has an average thickness of δ_{por} = 12.5 µm [4]. After the corrosion process starts, this porous area will gradually fill up with rust. When the amount of the rust will surpass the necessary amount to fill up this area completely, at $t = t_{stress}$, the radial expansion pressure will occur, therefore extending the damage to the adjacent layers of concrete. By calculating the corrosion current density <39> and the radial translocation of the rust expansion front <41>, the time necessary for the rust to fill the porous area around the reinforcement t_{stress} can be estimated.

Hot dip galvanized reinforcement

A layer of zinc was added to the steel beam, resulting a coating thickness of d = 140 µm. In calculating

the corrosion current density and the thermal conductivity coefficient of the galvanized reinforcement at the steel/concrete interface, necessary modifications were introduced. For the zinc, the following values were used: density ρ_z = 7140 kg/m^3, atomic mass m_{az} = 65.38 g/mol, valence v_z = 2, specific heat c_z = 390 J/kg°K, thermal conductivity k_z = 116 W/m°K and the thermal expansion coefficient ε = 30.2 µm/m°K. According to literature, the critical initial chlorine content for the corrosion process to take place, is $C_{LFzinc\text{-}critic}$ = 1.9 kg/m^3. The results obtained for the temporal and spatial distribution of temperature, moisture and chlorine content are not presented in this case, because they are not significantly influenced by the thin zinc layer, and are similar to those of the bare steel samples. The distribution of the parameters directly related to the corrosion process of the galvanized reinforcement are detailed.

3.7 Comparing the results obtained for the galvanized and bare steel reinforcements

Using results obtained for the corrosion current density, an efficiency index IE for corrosion inhibition through galvanized steel was calculated. The mathematical relation is often used in literature [8], according to equation <42>.

$$IE = \frac{i_{corr} - i^0_{corr}}{i_{corr}} \times 100\% \qquad <42>$$

$$IE = \frac{\sum_{k=1}^{75} i_{corr,k} - \sum_{k=1}^{75} i^0_{corr,k}}{\sum_{k=1}^{75} i_{corr,k}} \times 100\% \qquad <43>$$

where i_{corr} is the corrosion current density for the bare steel reinforcements, and i^0_{corr} is the corrosion current density for the galvanized steel. Considering that the numeric model provides these values on the discretized network cells, as shown in the previous sections, the corrosion current density is not evenly distributed along the reinforcement, in equation <42>, i_{corr} and i^0_{corr} were replaced with the sum of the values obtained in the adjacent cells of the reinforcement, according to relation <43>.

4 Results

To complete the experiment, calculations were made according to the theoretical model, imposing both initial conditions and, as boundary conditions, the data used to conduct the experiment in the laboratory. To emphasize the irregular distribution, both in space and time, of the temperature, moisture content and chlorine level in the concrete cells adjacent to the reinforcement, the following three points were chosen, noted as *A*, *B*, with the distances d_A = 1 mm, d_B = 70 mm between the points and the top side of the cubic concrete sample, and *C*, with the distance to the bottom side of the cubic concrete sample of d_C = 11 mm. During the simulation run, the values for the variables *T*, *w* and C_{LF} for each point are saved in separate files for each timeframe, for later processing.

The computer program used was written in the Delphi programming language.

4.1 Applying the numeric model for the galvanized reinforcement

Immersion in NaCl 3 %

The expansion front of the corrosion products is noticed only at the top end of the beam, for about 2 mm. This initiation appeared at $t = t_{stress}$ = 0,2687 years, meaning that approximately 98.1 days have passed since the immersion in 3 % NaCl solution. For about 2 mm along the top end of the beam, the diameter was reduced by $D_b - D_{rb}$ = 8 mm – 7,872357 mm = 0,127643 mm ≈ 127.6 µm, and from 2 to 4 mm from the end of the beam, by 2,2 µm.The diameter was reduced by under 0,1 µm along the rest of the affected beam. So, we can conclude that the zinc layer was only partially affected at the end of the experiment *(Fig. 9* and *10)*.

The decrease in diameter is not even along its length. Observe that the speed of diameter decrease reaches a maximum point at the top end of the beam, and then descends quickly towards the center of the cubic sample (*Fig. 10*). At the bottom end of the beam, the speed of the diameter decrease is lower at a distance of about 11 mm from the steel/NaCl solution interface, but has the same predisposition to slow down as it reaches the center of the sample.

The evolution of corrosion current density at the concrete/reinforcement interface, at the top end of the galvanized beam is presented in *Figure 11(a)*. Again, a rapid increase of i_{corr} in the first few days is noticed, then after the 17th day, when it reaches the value of 115 µA/cm^2, the process is slowed down, converging gradually to 119,12 µA/cm^2. Between 2

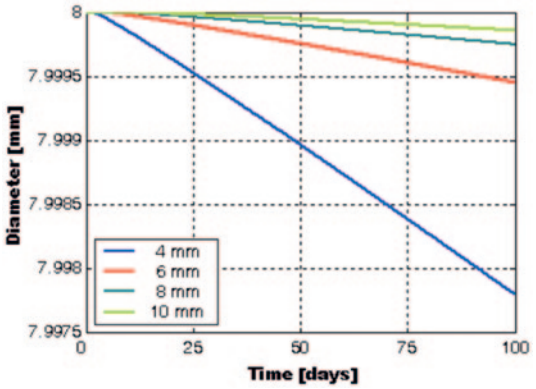

Fig. 9: The modifications of the galvanized reinforcement diameter (blue) and rust expansion front diameter (red) that take place in time, for a distance of 2 mm from the top end of the beam

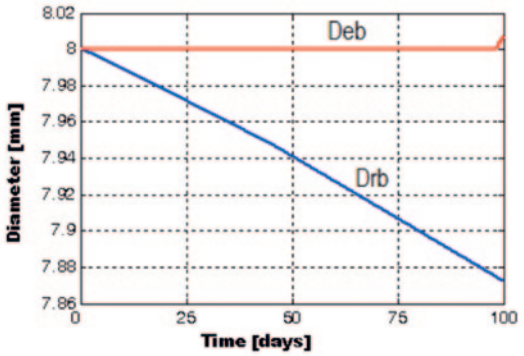

Fig. 10: The modifications of the galvanized beam's diameter that take place in time, at specified distances of 4, 6, 8 and 10 mm from the top end of the beam

and 10 mm from the top end of the beam, i_{corr} suddenly drops to 2.3 µA/cm^2 for the first 2 mm, and then under 0.7 µA/cm^2. In *Figure 11(b),* the corrosion current densities for the portions from 2 to 4 mm, 4 to 6 mm, 6 to 8 mm and 8 to 10 mm from the top end of the beam are shown. It proves that the time it takes for the corrosion process to initiate increases from the end of the beam to the center of the cubic sample, as the intensity of i_{corr} decreases. At the lower end of the beam, i_{corr} is still below 0.08 µA/cm^2 along the corrosion affected area.

The effect of the freeze-thaw cycles

In the case of the concrete sample reinforced with hot dip galvanized steel reinforcement, when subjected to freeze-thaw cycles, it is noted that the corrosion current only appears at the top end of the beam, for about 4 mm in length along the beam, and the lower end of the beam is not affected by corrosion. It may also be noticed that the sudden decrease of the corrosion current density for the area between 2 and 4 mm from the top end of the beam also takes values from 46.8 µA/cm^2 to 0.06 µA/cm^2.

The fluctuation of the galvanized reinforcement diameter (D_{rb}) is presented in *Figure 12.* At the end of the cycles, up to 2 mm from the top end of the beam, it's diameter has shrunk by 44.0 µm, that is 45.7 µm less shrinkage than the bare steel reinforcement. The corrosion process started during the first cycle. From 2 to 4 mm from the top end of the beam, the corrosion began 32.4 days after the first cycle began, and 100 days after the beginning of the freeze-thaw

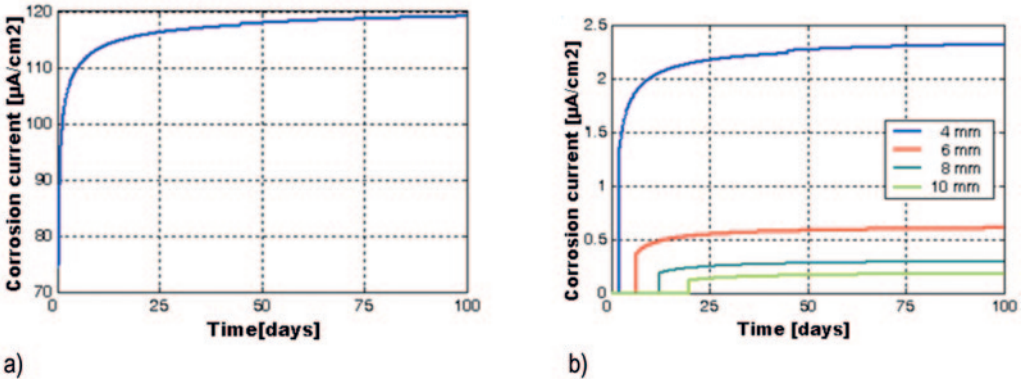

Fig. 11: Temporal variations of corrosion current density at 2 mm (a), 4, 6, 8 and 10 mm from the top end of the beam (b), at the concrete / reinforcement interface

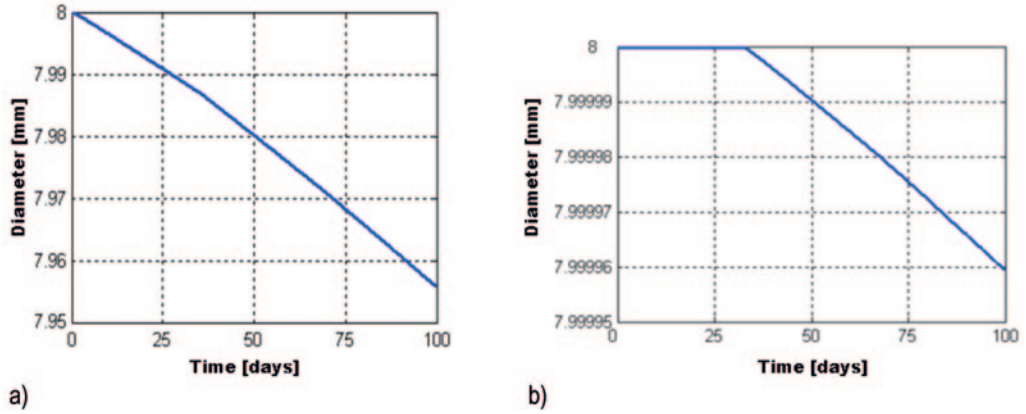

Fig. 12: The variation in time of the galvanized beam's diameter for the first 2 mm (a), and the area between 2–4 mm (b) from the top end of the beam

cycles, the diameter of the reinforcement shrunk by only 0.041 µm.

In *Figure 13*, the evolution of the corrosion current density is illustrated, for the areas between 0 and 2 mm and 2 to 4 mm from the top side of the beam. Notice that between 0 and 2 mm, the corrosion current density oscillates between 20 and 42 µA/cm^2 between cycles 3 and 35, after which an increase of the intensity is noticeable, as well as a decrease in the oscillations amplitude, which take values between 42 and 54 µA/cm^2.

4.2 Applying the numeric model for the bare steel reinforcement

Immersion in NaCl 3 %

The corrosion of the bare steel reinforcement was noticed for about 22 mm from the top end of the beam, and 10 mm from the lower end. Between 0 and 2 mm from the top, the diameter of the reinforcement was reduced by $D_b - D_{rb}$ = 8 mm – 7,856243 mm = 0,143767 mm ≈ 143.8 µm. This area is most affected by the chlorides, being closest to the side of the sample exposed to the NaCl solution. At distances of 4 and 6 mm from the top end, the difference $D_b - D_{rb}$ drops suddenly to 0.7 µm, respectively 0.1 µm, and for the rest of the affected portions – both at the top and bottom end of the beam – this difference remains under 0.1 µm.

The rust expansion front was initiated only at the top end of the beam, along a 2 mm distance. This initiation occurred at $t = t_{stress}$ = 0,0264 years = 9.6 days after the immersion in 3 % NaCl solution. This initiation time is relatively short because i_{corr} has higher values, at the end of the 100 days having reached 144,1 µA/cm^2.

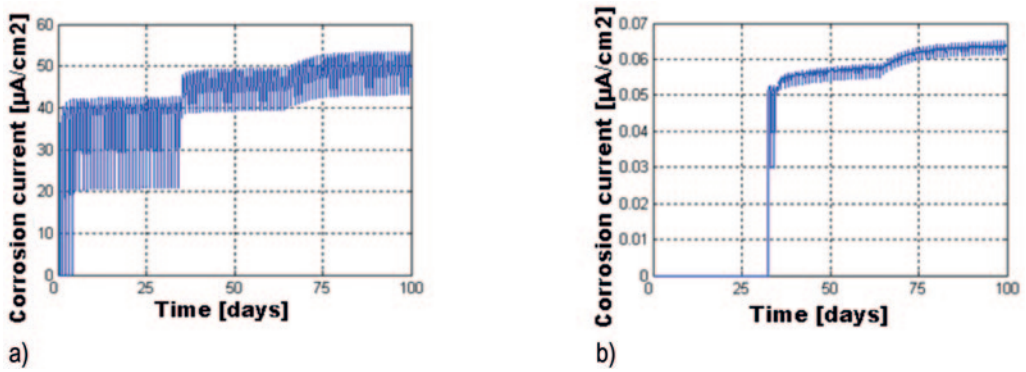

Fig. 13: The evolution of the corrosion current density, icorr, for the areas between 0–2 mm (a) and 2–4 mm (b) from the top end of the galvanized beam

Keep in mind that i_{corr} has lower values in other areas where the corrosion process of the steel was initiated. It must be pointed out that, in literature, when testing accelerated corrosion, high values of corrosion current densities are used. Therefore, Li and others (2005) [9], impose i_{corr} = 100 µA/cm² – along the full length of an L = 39 cm long reinforcement – and cracks in the concrete appear after less than 7 days due to the rust expansion front.

In *Figure 14*, the evolution of the corrosion current density at the concrete/reinforcement interface is shown, which influences the first 2 mm of the top end of the beam for 100 days after the immersion in 3 % NaCl solution, expressed in µA/cm². i_{corr} rapidly increases during the first few days, reaching a value of 140 µA/cm² after approximately 18 days, after which it slows down, tending to stabilize at around 144 µA/cm², probably due to the fact that the chlorine has reached maximum value.

The chart in *Figure 15* presents the fluctuation of the beam's diameter Drb, and the diameter of the radial rust expansion front Deb, at the superior level of the model (k = 76). Again, it is to be observed that in this area of the reinforcement – with the given conditions – a time period of 9 days is necessary ($t_{stress} - t_{initiere} \approx 9$ days) from the beginning of the corrosion process until the rust expansion starts.

The effect of the freeze-thaw cycles

Chlorine only affects the tips of the reinforcement. In point A, situated 1 mm above the top end of the beam, the oscillations that appear due to the immersion/extraction cycles in the chlorine solution can be distinguished. Starting with the 4th day, those oscillations have steady values between 2 and 3.8 kg/m³. To be noted that the critical chlorine content – necessary to start the corrosion process – is surpassed since the first freeze-thaw cycle.

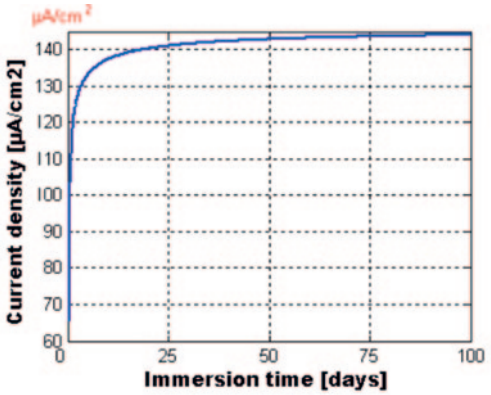

Fig. 14: The corrosion current density icorr [µA/cm²], at the concrete/reinforcement interface, 2 mm from the top end of the beam

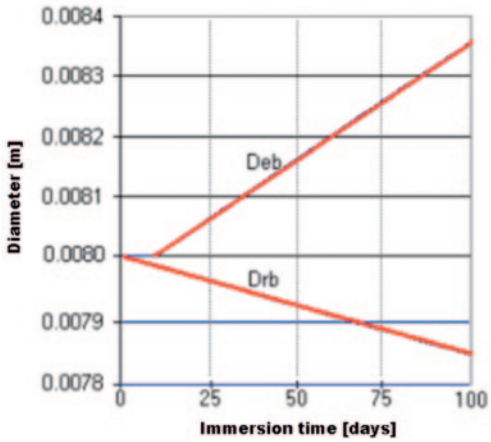

Fig. 15: Temporal evolution of the steel reinforcement diameter D_{rb}, and the expansion front D_{eb}, at the concrete/reinforcement interface, 1 mm from the top end of the beam

In point C, at 11 mm from the lower end of the beam, the oscillations mentioned above are not distinguished, and the maximum chlorine content is 0.82 kg/m³ at the end of the 100 days, so the critical chlorine level is not reached. Actually, during this experiment, the critical level is reached only for an 8 mm portion at the top end of the beam. The corrosion intensity is not distributed evenly on that area. The most considerable variations of the beam diameter and rust expansion front diameter were found in the first 2 mm, and on the next 6 mm these variations are a lot less significant, plus the expansion front has not appeared.

For a depth of about 2 cm below the top side of the concrete sample, corrosion in the reinforcement occurred during the first cycle, and the rust expansion began during the 16th cycle. At the end of the 100th cycle, D_{rb} has decreased by 89.7 µm, and D_{eb} has increased by 211.8 µm (*Fig. 16*). The corrosion current density oscillated due to the NaCl solution immersion/extraction cycles. The amplitude of these oscillations is not evenly distributed on the area affected by corrosion. The value of the corro-

sion current i_{corr} is 41 to 93 µA/cm² at the beginning, then gradually increases and stabilizes between 52 and 107 µA/cm². The amplitude of these oscillations gradually increases from 48 to 54 µA/cm².

Between 2 and 4 mm from the top end of the beam, the corrosion process first occurred during the 10th cycle, and the intensity of i_{corr} abruptly decreases until it reaches 0.09–0.21 µA/cm². The oscillations are greatly reduced, the amplitudes taking values between 0.07 µA/cm² at the beginning of the corrosion process, and 0.009 µA/cm² at the end of the trial period *(Fig. 17)*.

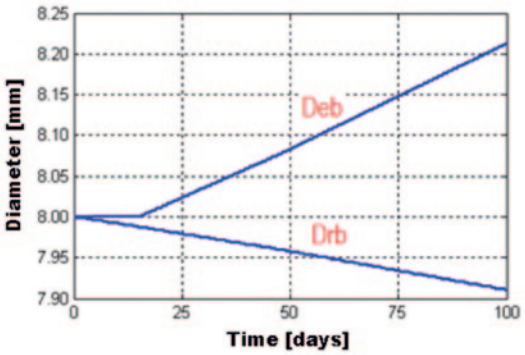

Fig. 16: Evolution of the steel reinforcement diameter and the rust expansion front diameter, 2 mm from the top end of the beam

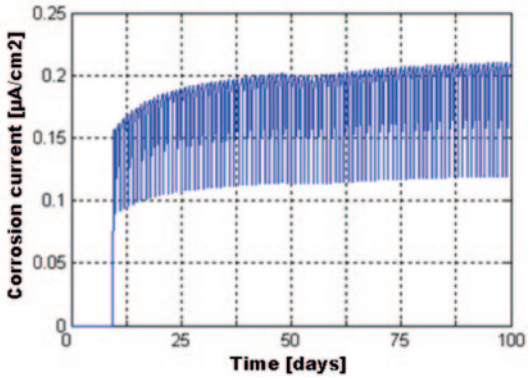

Fig. 17: Evolution of the corrosion current density, 2–4 mm from the top end of the beam

4.3 Experimental verification of the numeric model

The reduction of the adherence between reinforcement and concrete was calculated as the difference between the initial adherence (control sample) and the final adherence (the sample subjected to negative conditions) – *Table 1*, based on the experimental data.

Based on the elasticity theory of concrete and by considering that the internal pressure caused by the radial expansion of the volume of corrosion products in the reinforcement is directly responsible for the decrease in adherence between reinforcement and concrete according to the model presented by Ugual [16, 17], adapting it to the situation at hand, as shown in equation <44>.

$$p_{cor} = \frac{2 \cdot E \cdot \alpha}{(R_2 + 2 \cdot \delta_{por}) \cdot \frac{b^2 + a^2}{b^2 - a^2}} \qquad <44>$$

where

E = modulus of elasticity in concrete

α = the radial expansion of the corrosion products layer

R = the initial radius of the reinforcement, considered a perfect cylinder

δ_{por} = the thickness of the porous layer located at the concrete reinforcement interface is – according to specific literature – 12,5 µm

b = the external radius of the concrete cylinder, with the thickness L

a = The internal radius of the concrete cylinder, with the thickness L

Considering the fact that the radial expansion of the corrosion products layer is half of expansion front's diameter D_{eb}, determined for the galvanized and bare steel, according to the proposed numeric model, the decrease of adherence between reinforcement and concrete was calculated as being equal to the internal strain caused by the radial expansion of the corrosion layer.

Tab. 1: IE index values (%)

Experiment	*IE (%)*
28 days laboratory conditions, followed by maintaining for 100 days in NaCl 3 % solution	15.7
28 days laboratory conditions, followed by maintaining for 25 days in NaCl 3 % solution	15.8
28 days laboratory conditions, followed by 100 days of frost – defrost cycles	42.9
28 days laboratory conditions, followed by 25 days of frost – defrost cycles	43.5

The decrease of the adherence between the reinforcement and concrete, determined both experimental and due to the numeric model, is presented in *Figure 18*. By calculating the standard error between the results obtained during the experiment and as a result of the numeric modelling, these models are correlated.

4.4 Comparing the results obtained for the galvanized and bare steel reinforcement

The values for the corrosion inhibition index for the hot dip galvanized and bare steel reinforcements are compared in *Table 1*. These values were calculated based on the results obtained during the laboratory experiments.

During the freeze-thaw cycles, the inhibition efficiency is greater IE = 42.9%, than the IE = 15.7% obtained by maintaining the cubic sample in 3% NaCl solution for 100 days, where we may also note that IE slightly decreases the longer the sample was immersed in the solution.

The IE index varies, as shown in *Figure 19*.

5 Summary

The mathematical modelling based on the electrochemical phenomenon that takes place uses discretization methods of the physical element. A numerical model was conceived in order to simulate the main physical phenomena that influence corrosion in reinforced concrete.

The results of the numeric simulation show clearly that by galvanizing the steel reinforcements, corro-

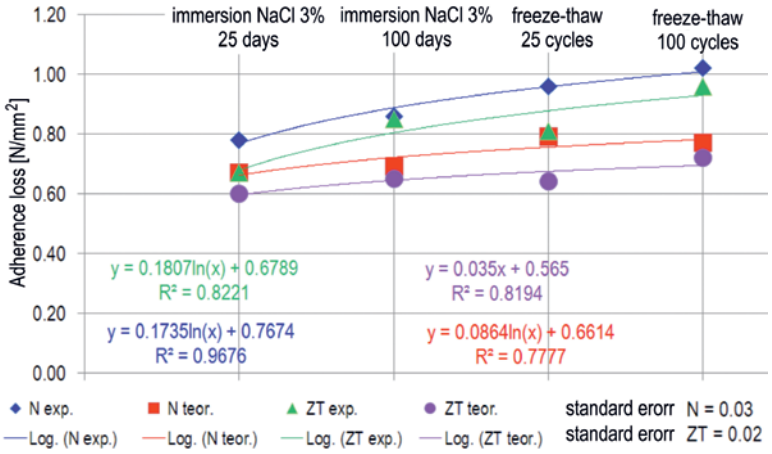

Fig. 18: Verification of the proposed theoretical model for the corrosion of hot dip galvanized (ZT) and bare (N) steel in concrete

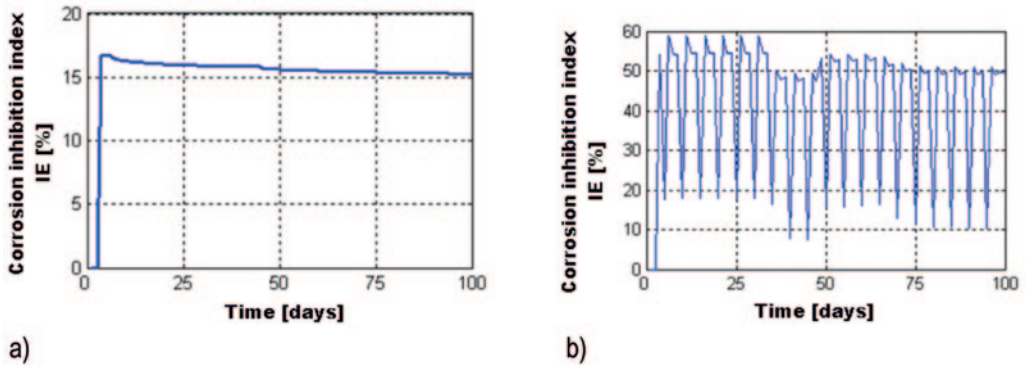

Fig. 19: Variation of the IE index when maintaining the sample for 100 days in 3% NaCl solution (a) and during 100 frost – defrost cycles (b)

sion process are inhibited, increasing the durability of reinforced concrete.

- The shrinking rate of the reinforcement's diameter is lower in the case of hot dip galvanized reinforcements, in similar aggressive environments and time of exposure. So, for a distance of 2 mm from the top end of the galvanized beam, the diameter shrunk by ≈ 127.6 µm, unlike the plain beam, which shrunk by 143,8 µm.
- It takes longer for the corrosion process to begin in similar aggressive environments and time of exposure for the galvanized reinforcement. The rust expansion front originated at the top end of the bare steel beam, along an area of 2 mm, in 0.0264 years, which means approximately 9.6 days after the immersion in 3 % NaCl solution. For the galvanized beam, the expansion front of the corrosion products originated at the top end of the beam along a portion of 2 mm in 0.2687 years, which means 98.1 days after the immersion. The difference between the two periods of rust expansion front occurrence is extremely significant, about 88.5 days.
- Due to its high values, the corrosion current indicates a much greater speed for the corrosion of the bare steel beam, compared to the galvanized reinforcement.
- A slight decrease of the IE index in relation with the immersion period is noted when maintaining for 100 days in NaCl solution. In the case of freeze-thaw cycles, a greater fluctuation appears related to time, still the average of the IE values remains higher, IE = 42.9. So, inhibiting corrosion during the freeze – thaw cycles by using hot dip galvanized reinforcements is more efficient.

This mathematical model could give us a image of what evolves the adherence between the reinforcement and concrete, over a period of time extended to 20, 30, 50 years. This informations could be useful for the design of reinforced concrete structures and building sustainability assessment. By extending the mathematical model we can understand the corrosion behavior of steel reinforcement in real concrete structures. Is necessary to continue experimental testing for models of structures and transfer from laboratory tests at the in-situ tests.

Acknowledgements

This paper was supported by the project "Project development of doctoral studies in advanced technologies – PRODOC" contract no. POSDRU 6/1.5/S/5 and "Improvement of the doctoral studies quality in engineering science for development of the knowledge based society-QDOC" contract no. POSDRU/107/1.5/S/78534, projects co-funded by the European Social Fund through the Sectorial Operational Program Human Resources 2007-2013.

References

[1] Z. P. Bažant, J. C. Chen, A. M. Rosenberg, J. M. Gaidis 71(1988)9, Mathematical Model for Freeze-Thaw Durability of Concrete, Journal of the American Ceramic Society, pp. 776 – 783

[2] S. X. C. Cai, Y. Xi 3(2006)4, Parallel Finite Element Method for Coupled Chloride Moisture Diffusion in Concrete, International Journal of Numerical Analysis and Modeling, pp. 481 – 503

[3] D. Chen, C. Liu, Q. Chunxiang 4(2009)5 Numerical experiment on hygro-thermal deformation of concrete with different material or structural parameters, International Journal of Physical Sciences, pp. 354 361, ISSN 1992 - 1950

[4] D. Chen, S. Mahavedan 30(2008) Chloride-induced reinforcement corrosion and concrete cracking simulation, Cement & Concrete Composites, pp. 227 – 238

[5] Y. Chen, S. Sun, Y. Liu (2007) Numerical Simulation of the Mechanical Properties and Failure of Heterogeneous Elasto- Plastic Materials, Tsinghua Science and Technology, Vol 12, No. 5, pp. 527 – 532, ISSN 1007-0214 04/19

[6] L. Daigle, Z. Lounis, D. Cusson (2004) Numerical prediction of early-age cracking and corrosion in high performance concrete bridges – case study, Proceedings of the TAC Annual Conference – Transportation Innovation-Accelerating the Pace, Quebec City, Canada, pp. 1 – 20

[7] D. Ferretti, Z. P. Bažant 36(2006)9 Stability of ancient masonry towers: Moisture diffusion, carbonation and size effect, Cement and Concrete Research, pp. 1379 – 1388

[8] O. A. Hazzazi 37(2007) Corrosion inhibition studies of copper in highly concentrated NaCl solutions, Journal of Applied Electrochem, pp. 933 – 940

[9] C. Q. Li, W. Lawanwisut, J. J. Zheng, W. Kijawatworawet 3(2005)2 Crack Width Due to Corroded Bar in Reinforced Concrete Structures, International Journal of Materials & Structural Reliability, pp. 87 - 94

[10] Y. Liu, R. E. Weyers 28(1998)3 Modeling the dynamic corrosion process in chloride contanimated concrete structures, Cement and Concrete Research, pp. 365 – 379

[11] X. Ma, B. Cheng, J. Mao, W. Liu, D. Zi (2009) Finite element modelling of coupled heat and moisture transfer in typical earth-sheltered building envelope, Proceedings of the Eleventh International IBPSA Conference, Glasgow, Scotland, Building Simulation, pp. 1850 – 1856

[12] S. V. Patankar (1980) Numerical Heat Transfer and Fluid Flow, Taylor & Francis, New York

[13] C. E. Zhou, F. J. Vecchio 2(2005)6 Nonlinear finite element analysis of reinforced concrete structures subjected to transient thermal loads, Computers and Concrete, pp. 455 - 479

[14] Y. Xi, Z. P. Bažant 11(1999)1 Modeling Chloride Penetration in Saturated Concrete, Journal of Materials in Civil Engineering, pp. 58 – 65, ISSN 0899-1561/99/0001

[15] Y. Xi, Z. P. Bažant, H. M. Jennings (1994)1 Moisture diffusion in cementitious materials – adsorption isotherms, Advanced Cement Based Materials, pp. 258 – 266

[16] Ugual A.C., Advanced strength and applied elasticity. London, Elsevier Applied Science (1986)

[17] Liang. M. T., Yang. R. J. Theoretical elucidation on the on-site measurement of corrosion rate of reinforcement, Construction and Building Materials 19, Science Direct, Elsevier (2005) pp. 175-180